scientific reports

Check for updates

OPEN

Controlled synchronization of three co-rotating exciters based on a circular distribution in a vibratory system

Lei Jia[1]✉, Yang Tian[2], Ziliang Liu[1] & Xin Zhang[1]

In this article, an engineering problem of three co-rotating exciters with the circular distribution in a vibrating system is investigated. The dynamical model constructed by the motion differential equations is established. By introducing the small parameter averaged method in the dynamic equation, the synchronization and stability conditions of the electromechanical coupling dynamical model is derived. To illustrate the necessity of the controlling method, the self-synchronization of the vibrating system is firstly analyzed with the theory, numerical simulations and experiments. With the self-synchronization results, it is indicated that the ellipse trajectory which is needed in the industry can't be realizefd by the self-synchronization motion of the vibrating system. And then, a fuzzy PID controlling method based on the master–slave controlling strategy is introduced in the vibrating system to realize the controlled synchronization. The Lyapunov stability criterion is given to certify the stability of the controlling system. Through some simulations and experiments, the effectiveness of controlled synchronization is illustrated in the discussion. Finally, the present work illuminates the feasibility and practicality for designing some new types of vibrating screens in the industry.

Keywords Self-synchronization, Controlled synchronization, Coupling dynamical model, Vibratory system, Exciter rotors

Nowadays, the vibratory machinery has a rapid development with an improvement of the technology in the industry, for example the vibrating screen, vibrating feeder and so on[1–3]. The vibrating screen is used in various of industry fields because of its large potential economic benefits. The actuators of the vibrating screen with traditional forms usually adopt the forced synchronization motion by gears, belts, chains or some other transmission mechanisms. However, the more mechanism parts are used, the lower reliability the vibrating system is. This result could decrease the useful life of the vibrating system. With the development of the synchronous theory, some synchronous methods are presented by the dynamical intrinsic character. The theory of vibration synchronization is firstly represented by Blekhman et al.[4,5] In their work, two eccentric rotors (ERs) separately driven by two motors are installed on a vibrating bench with the same frequency. They divide the motion of the vibrating system into two processes with different time scales. One is the faster process and the other is lower process. With this method, they obtain the synchronization and stability conditions of two motors rather than the coupling characteristics of the vibrating system. Inoue et al.[6] realizes the self-synchronization motion of two and three times frequency with four motors. Wen et al.[7] have research on the self-synchronization motion with two motors in a vibrating system. In the research, the synchronization and stability conditions of the whole vibrating system is derived with the average method and Hamilton principle. Zhao et al.[8,9] proposes the small parameter average method based on the perturbation method. And with this method, they substitute the problem of synchronization for existence and stability of the eigenvalues which are obtained from the dynamical equations of the vibrating system. Zhang et al.[10–12] not only establishes the dynamical model of three motors in a vibrating system, but also provides the experiment results of the self-synchronization. In the meanwhile, the double and triple frequency synchronization is studied. In their research work, the synchronous and stability conditions of the vibrating system with three ERs are derived and the results show that when the synchronous and stability conditions are not satisfied, the circular motion which is needed in the vibratory screen can't be realized. Balthazar et al.[13,14] analyze the problem of self-synchronization with four direct current (DC) motors.

[1]School of Mechanical Engineering, Shenyang Ligong University, Shenyang 110159, China. [2]School of Mechanical Engineering, Liaoning Engineering Vocational College, Tieling 112008, China. ✉email: jialeizsq@126.com

They use the elastic support to replace the rigid body and introduce the numerical method into the dynamical model instead of the analytical solution.

As illustrated above, the self-synchronization motion should satisfy the synchronous and stability conditions so that it can realize the needed trajectory in the vibratory screen. Aim at this problem of the self-synchronization, the method of controlled synchronization which introduces the controlling method and controlling strategy into the self-synchronization is presented. Kong et al.[15–17] realizes the controlled synchronization motion of three and four ERs in a vibrating system. The master–slave controlling strategy is used in the controlled system with the adaptive slide controlling method. Besides that, the synchronization based on an elastic beam is also studied. In their work, the approximate circular trajectory is realized with three ERs driven by inductor motors which are installed in one line on a rigid frame. And then, the linear trajectory is given with four ERs driven by inductor motors which are symmetrically installed along the horizontal and vertical axes. Perez-Pinal et al.[18] represents a controlling strategy titled relative coupling control. Huang et al.[19,20] introduces the relative coupling controlling method into a non-linear vibrating system and realizes the controlled synchronization motion with two ERs. The multifrequency synchronization with controlling method is studied. Priyanka et al.[21] uses the fuzzy PID controlling method to realize the fluid machinery control, which provides a way for the controlled synchronization. Jia et al.[22,23] use the controlled synchronization and composite synchronization method on the multifrequency synchronization motion. In their research, the non-integer multifrequency controlled synchronization is investigated.

Compared with the finished research work, it can be known that the self-synchronization with three ERs can't realize the approximate circular trajectory which can be realized by controlled synchronization method. However, the ERs driven by inductor motors with the linear distribution need a larger frame. This result may not be suit for some smaller vibratory screen. Thus, an engineering problem of three co-rotating exciters with the circular distribution in a vibrating system is investigated. The structures of present work are as follows: the electromechanical coupling dynamic model of the vibrating system is established in Section "Synchronization and stability analysis of dynamical differential equation". And then the motion differential equation of the dynamic model is derived. The synchronous and stability conditions of the self-synchronization with three ERs is obtained. In Section "Design and theoretical analysis of the controlling system", the controlling method is introduced to establish the controlling system and the stability of the controlling system is certified by the Lyapunov criterion. Section "Results analysis and discussions" shows the discussions with theory, numerical simulations and experiments. Finally, some conclusions are summarized in Section "Conclusions".

Synchronization and stability analysis of dynamical differential equation

The establishment of the theoretical model

The model of the vibratory screen can be simplified as the theoretical model of a vibrating system shown in Fig. 1. And the significance of mathematical symbols in this paper are all listed in Table 1. The vibrating system is constructed from top to the bottom. Two inductor motors with ERs are symmetrically installed on a rigid frame along the vertical axis. One motor is installed under the rigid frame on the vertical axis. $o_i(i=1,2,3)$ are respectively the rotating center of three ERs. The frame is supported by four springs which provide the stiffness in the x and y directions. o is the center of the rigid frame. M is the total mass of the vibrating system, $M = m + m_i(i = 1, 2, 3)$. m is the mass of the frame and $oo_i = l_i(i = 1, 2, 3)$. J and J_p are respectively the inertia moment of the vibrating system and the rigid frame, $J = Ml_e^2 \approx J_p + \sum_{i=1}^{3} m_i(l_i^2 + r^2)$. l_e is equivalent rotation radius. f_x, f_y and f_ψ are the damping coefficients, $f_\psi = l_0^2(f_x \sin^2\beta + f_y \cos^2\beta)$. k_x, k_y and k_ψ are the stiffnesses, $k_\psi = l_0^2(k_x \sin^2\beta + k_y \cos^2\beta)$. f_i $(i=1,2,3)$ respectively represents damping coefficients of the inductor motor. The parameters of the vibrating system are given in Table 2.

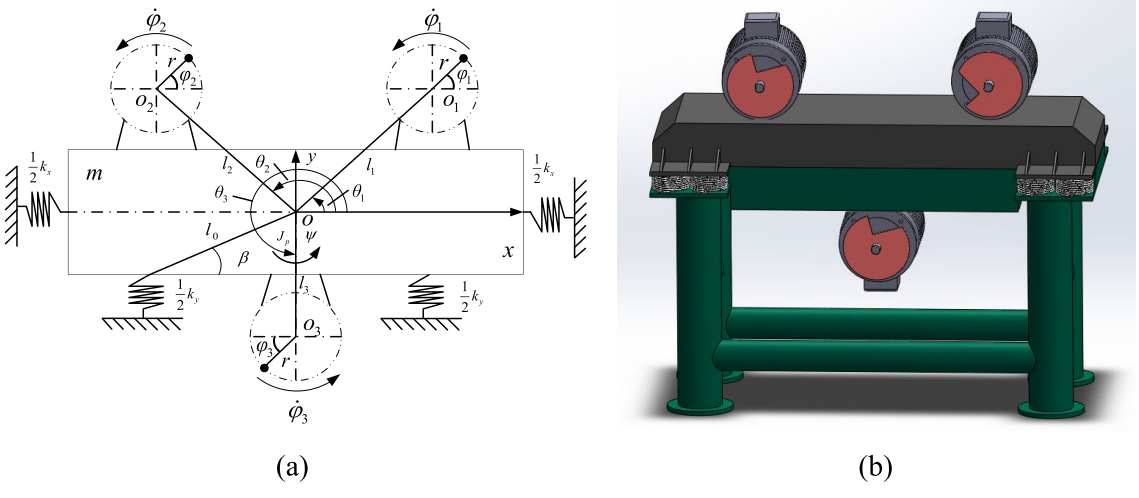

Figure 1. Mathematical model of the vibrating system.

Symbol	Significance
m_i	The mass of each ERs
J_p	The moment of inertia of the rigid frame
J	The moment of inertia of the vibrating system
k_x, k_y, k_ψ	The stiffness coefficients of the vibration system in the x, y and ψ directions
r	The eccentric radius of the inductor motors
M	The total mass of the vibration system
f_x, f_y, f_ψ	The damping coefficients of the vibration system in the x, y and ψ directions
l_1, l_2, l_3	The distance between the center of the body and the rotating center of motors
J_i	The moment of inertia of the inductor motor
d-, q-	The d- and q- axes in rotor field-oriented coordinate
L_s	Self-inductance of the stator
L_r	Self-inductance of the rotor
Subscript s	Stator
Subscript r	Rotor
L_m	Mutual inductance of the stator and rotor
L_{ks}	Leakage inductance of the stator
ϕ_{sd}	The flux linkages of the stator in the d- axis
ϕ_{sq}	The flux linkages of the stator in the q- axis
ϕ_{rd}	The flux linkages of the rotor in the d- axis
ϕ_{rq}	The flux linkages of the rotor in the q- axis
R_s	The stator resistance
R_r	The rotor resistance
R_{ks}	Equivalent resistance of the stator
i_{sd}	The current of stator in the d- axis
i_{sq}	The current of stator in the q- axis
i_{rd}	The current of rotor in the d- axis
i_{rq}	The current of rotor in the q- axis
ω	The mechanical speed
ω_s	The synchronous electric angular speed
$\dot{\phi}_{sd}$,$\dot{\phi}_{sq}$,$\dot{\phi}_{rd}$,$\dot{\phi}_{rq}$	Derivation ofϕ_{sd},ϕ_{sq},ϕ_{rd},ϕ_{rq}
σ	The leakage factor
Tr	A rotor time constant
u_{sd}	The voltage of stator in the d- axis
u_{sq}	The voltage of stator in the q- axis
u_{rd}	The voltage of rotor in the d- axis
u_{rq}	The voltage of rotor in the q- axis
n_p	The number of pole-pairs of the induction motor
$\bullet^*$	The given values or obtained from the given values
ω_1,ω_2,ω_3	The speeds of three motors
φ_1,φ_2,φ_3	The phases of three motors
θ	Synchronization electric angle

Table 1. The nomenclature table of the symbols.

According to Fig. 1, the mathematical model of the vibrating system can be derived with Lagrange equation.

$$\frac{\mathrm{d}}{\mathrm{d}t}\left(\frac{\partial(T-V)}{\partial\dot{\mathbf{q}}}\right)-\frac{\partial(T-V)}{\partial\mathbf{q}}+\frac{\partial D}{\partial\dot{\mathbf{q}}}=\mathbf{Q} \tag{1}$$

Equation 1 contains four variables, the first is the kinetic energy T which is composed of three parts. They are respectively the item of translational energy of the rigid body $T_{teb}=m(\dot{x}^2+\dot{y}^2)/2$, rotational energy of the rigid body $T_{reb}=J_b\dot{\psi}^2/2$ and the kinetic energy of three ERs $T_{kee}=\left(\sum_{i=1}^{3}m_i\dot{\delta}_i^{\mathrm{T}}\dot{\delta}_i+\sum_{i=1}^{3}J_i\dot{\varphi}_i^2\right)/2$, where, $\delta_i=\delta_0+\chi\delta_i''$. According to the transformation of the coordinate system, it can be derived as $\delta_0=\begin{pmatrix}x\\y\end{pmatrix}$, $\chi=\begin{pmatrix}\cos\psi & -\sin\psi\\ \sin\psi & \cos\psi\end{pmatrix}$, $\delta_i''=\begin{pmatrix}l_i\cos\theta_i+r\cos\varphi_i\\ l_i\sin\theta_i+r\sin\varphi_i\end{pmatrix}$. Thus, the total kinetic energy of the system can be expressed

Parameters	Values
M /kg	304
J_p /(kg.m^2)	44.5
k_x /(N/m)	129,332
k_y /(N/m)	105,334
k_ψ /(Nm/rad)	30,715
f_x /(Ns/m)	615.5
f_y /(Ns/m)	618
f_ψ /(Nsm/rad)	180.2
$\theta_1, \theta_2, \theta_3$ /(°)	30, 150, 270
m_0 /kg	6
r /m	0.05
l_1, l_2, l_3 /m	0.45, 0.45, 0.36

Table 2. The parameters of the vibrating system.

as $T = T_{teb} + T_{reb} + T_{kee}$. The second is the potential energy V which can be expressed as $V = (k_x x^2 + k_y y^2 + k_\psi \psi^2)/2$. The third is the energy dissipation D described as $D = \left(f_x \dot{x}^2 + f_y \dot{y}^2 + f_\psi \dot{\psi}^2 + \sum_{i=1}^{3} f_i \dot{\varphi}_i^2\right)/2$. The last items are the generalized force $\mathbf{Q} = (Q_x, Q_y, Q_\psi, Q_1, Q_2, Q_3)^{\mathrm{T}} = (0, 0, 0, T_{e1}, T_{e2}, T_{e3})^{\mathrm{T}}$ and the generalized coordinate $\mathbf{q} = (x, y, \psi, \varphi_1, \varphi_2, \varphi_3)^{\mathrm{T}}$. Through Eq. (1), the differential equations of the electromechanical coupling dynamical model can be expressed as Eq. (2) with the Lagrange function.

$$\begin{aligned}
&M\ddot{x} + f_x\dot{x} + k_x x = \sum_{i=1}^{3} m_i r\left(\dot{\varphi}_i^2 \cos\varphi_i + \ddot{\varphi}_i \sin\varphi_i\right)\\
&M\ddot{y} + f_y\dot{y} + k_y y = \sum_{i=1}^{3} m_i r\left(\dot{\varphi}_i^2 \sin\varphi_i - \ddot{\varphi}_i \cos\varphi_i\right)\\
&J\ddot{\psi} + f_\psi\dot{\psi} + k_\psi \psi = \sum_{i=1}^{3} m_i r l_i\left[\dot{\varphi}_i^2 \sin(\varphi_i - \theta_i) - \ddot{\varphi}_i \cos(\varphi_i - \theta_i)\right]\\
&J_i\ddot{\varphi}_i + f_i\dot{\varphi}_i = T_{ei} - T_{Li},\ \ i = 1, 2, 3
\end{aligned} \tag{2}$$

where, T_{Li} is the torque loads of three motors and it can be derived as Eq. (3).

$$T_{Li} = m_i r[\ddot{y}\cos\varphi_i - \ddot{x}\sin\varphi_i + l_i\dot{\psi}^2\sin(\varphi_i - \theta_i) + l_i\ddot{\psi}\cos(\varphi_i - \theta_i)] \tag{3}$$

The item T_e in Eq. (2) is the electromagnetic torque of the inductor motor. Thus, the model of the inductor motor should be established. In this article, the category of the inductor motor is the squirrel-cage motor. According to the feature of this kind of motor, its rotor winding is short circuit, which can be expressed as the mathematical form, $u_{rd} = u_{rq}$. When the motor is at a stable state, ϕ_{rd} = constant and $\phi_{rq} = 0$. With the variables ω-i_s-ϕ_r, the model of inductor motor in the d-q rotating coordinate system can be represented as Eq. (4) by literature[24].

$$\begin{aligned}
&L_{ks}di_{sd}/dt = u_{sd} - R_{ks}i_{sd} + R_r L_m/L_r^2\phi_{rd} + \omega_s L_{ks} i_{sq}\\
&L_{ks}di_{sq}/dt = u_{sq} - R_{ks}i_{sq} - L_m/L_r\phi_{rd}\omega - \omega_s L_{ks} i_{sd}\\
&d\phi_{rd}/dt = 1/T_r(L_m i_{sd} - \phi_{rd})\\
&d\theta/dt = L_m i_{sq}/T_r\phi_{rd} + \omega\\
&T_e = 3L_m\phi_{rd}i_{sq}/2L_r
\end{aligned} \tag{4}$$

The symbols in Eq. (4) are all given in Table 1. L_{ks} and R_{ks} respectively represent the leakage inductance and the equivalent resistance of the stator which can be derived as $L_{ks} = L_s - L_m^2/L_r$ and $R_{ks} = R_s + L_m^2 R_r/L_r^2$. θ and ω_s can respectively be represented with the mathematical formulation $\theta = \int(\omega + \omega_s)dt$ and $\omega_s = L_m i_{sq}/\phi_{rd}T_r$. To sustain the stability of the motor speed, the rotor flux-oriented control (RFOC) is introduced in the system which is shown in Fig. 2. In the meanwhile, the parameters of three motors are shown in Table 3.

The analysis of synchronization and stability of the vibrating system

According to the non-linear dynamical theory, the phase difference between motor 1 and 2 can be expressed as $p\varphi_1 - q\varphi_2 = 2\alpha_1$, and the phase difference between motor 2 and 3 can be expressed as $q\varphi_2 - s\varphi_3 = 2\alpha_2$. Set the average phase of three ERs as φ which can be represented as $\varphi = (\varphi_1 + \varphi_2 + \varphi_3)/3$. And then the average speed ω_0 in the period T can be derived as $\omega_0 = \int_0^T \dot{\varphi}dt/T$. With the small parameter method, the speed and accelerated

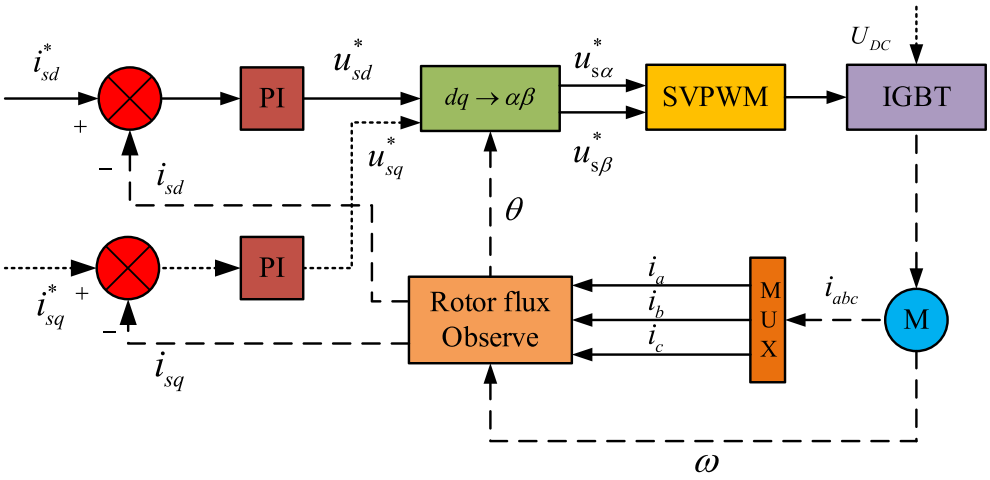

Figure 2. RFOC: rotor flux-oriented control.

Parameters	Motor 1	Motor 2	Motor 3
P /kW	0.2	0.2	0.2
n_p	3	3	3
f_0 /Hz	50	50	50
U /V	220	220	220
n /(r/min)	950	950	950
R_s /Ω	40.5	40.5	40.5
R_r /Ω	12	12	12
L_s /H	1.21275	1.2175	1.21275
L_r /H	1.222	1.225	1.222
L_m /H	1.116	1.116	1.116
λ_{dr}^*/Wb	0.98	0.98	0.98
$f_{1,2,3}$ /(Nms/rad)	0.005	0.005	0.005

Table 3. The parameters of three motors.

speed of three ERs are respectively $\dot{\varphi}_i = (1+\varepsilon_i)\omega_0$ and $\ddot{\varphi}_i = \dot{\varepsilon}_i\omega_0$, $i=1,2,3$. ε_i is the small perturbation parameter. ω_0 that is the mean value of the average speed of three motors equals to a constant. Then, the responses in three directions can be derived as Eq. (5)

$$\begin{aligned} x &= \frac{-r_m r}{\mu_x}\left[\sum_{i=1}^{3}\eta_i\cos(\varphi_i+\gamma_x)\right] \\ y &= \frac{-r_m r}{\mu_y}\left[\sum_{i=1}^{3}\eta_i\sin(\varphi_i+\gamma_y)\right] \\ \psi &= \frac{-r_m r}{\mu_\psi l_e}\left[\sum_{i=1}^{3}\eta_i r_{li}\sin(\varphi_i-\theta_i+\gamma_\psi)\right] \end{aligned} \tag{5}$$

where, $\omega_x^2 = k_x/M$, $\omega_y^2 = k_y/M$, $\omega_\psi^2 = k_\psi/J$, $\xi_x = f_x/\left(2\sqrt{k_xM}\right)$, $\xi_y = f_y/\left(2\sqrt{k_yM}\right)$, $\xi_\psi = f_\psi/\left(2\sqrt{k_\psi J}\right)$, $\tan\gamma_x = 2\xi_x\omega_x/(\mu_x\omega_0)$, $\tan\gamma_y = 2\xi_y\omega_y/\left(\mu_y\omega_0\right)$, $\tan\gamma_\psi = 2\xi_\psi\omega_\psi/\left(\mu_\psi\omega_0\right)$, $\mu_x = 1-\omega_x^2/\omega_0^2$, $\mu_y = 1-\omega_y^2/\omega_0^2$, $\mu_\psi = 1-\omega_\psi^2/\omega_0^2$, $r_m = m_0/M$, $\eta_i = m_i/m_0$, $r_{li} = l_i/l_e$.

From the equations above, the feature of the parameters r_{li}, r_m, and l_i are analyzed in the situation $l_1 = l_2 = l_3$. And then, the relationships among the three parameters are illustrated with different parameter η_i in Fig. 3. The results represent that the closer the masses of three ERs are, the better their synchronous capability is.

Taking the small parameters into Eq. (2), Eq. (6) can be obtained with the integrate method in the 2π period.

$$J_i\dot{\bar{\varepsilon}}_i\omega_0 + f_i\omega_0(1+\bar{\varepsilon}_i) = \overline{T}_{ei} - \overline{T}_{Li}(i=1,2,3) \tag{6}$$

where, the torque loads in Eq. (6) can be expressed with small parameters as

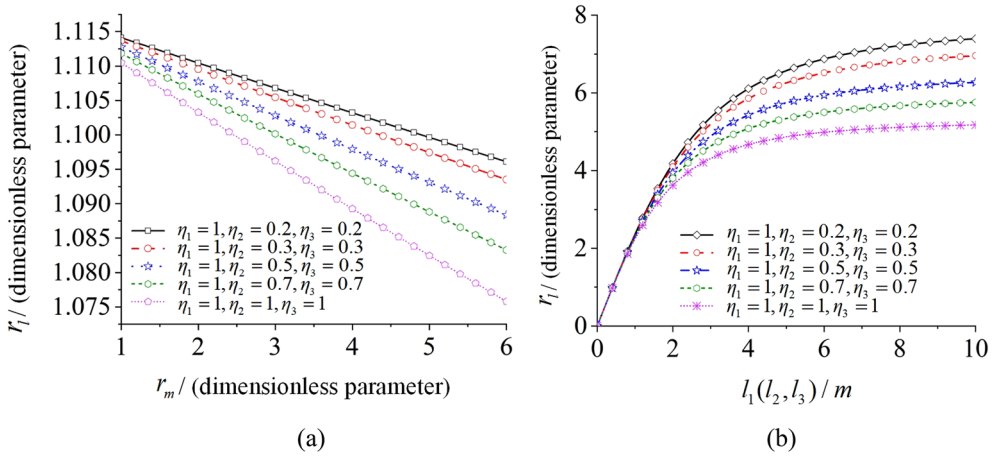

Figure 3. The feature analysis of three parameters.

$$\overline{T}_{Li} = m_0 r^2 \omega_0 \left[\sum_{j=1}^{3} (a_{ij}\dot{\overline{\varepsilon}}_j + b_{ij}\overline{\varepsilon}_j) + \kappa_i \right] (i = 1, 2, 3) \tag{7}$$

The items a_{ij}, b_{ij} and κ_i which are the second stability coefficient in Eq. (7) are all given in Appendix A. Because a_{ij} and b_{ij} are both associated with r_{li}, Fig. 4 shows their relationship feature with different parameter η_i. The results indicates that the parameters a_{ij} and b_{ij} are changed with the various parameter η_i and the coupling dynamical feature of the vibrating system demonstrates the best stable capability in the situation $\eta_1 = \eta_2 = \eta_3$. By introducing in the small parameter ε_4 and ε_5, expand the phase differences with the Taylor formula separately and omit the higher order items, $\alpha_1 = \overline{\alpha}_1 + \overline{\varepsilon}_4$ and $\alpha_2 = \overline{\alpha}_2 + \overline{\varepsilon}_5$ can be obtained. In the meanwhile, the non-dimensional coupling equations which is numbered as (8) can be derived as

$$\mathbf{A}\dot{\overline{\varepsilon}} = \mathbf{B}\overline{\varepsilon} + \boldsymbol{\upsilon} \tag{8}$$

where, $\mathbf{A}$ is a matrix of the moment of inertia and $\mathbf{B}$ is a stiffness matrix. The symbols in Eq. (8) are listed as below.

$$\mathbf{A} = \begin{pmatrix} a'_{11} & a'_{12} & a'_{13} & 0 & 0 \\ a'_{21} & a'_{22} & a'_{23} & 0 & 0 \\ a'_{31} & a'_{32} & a'_{33} & 0 & 0 \\ 0 & 0 & 0 & 1 & 0 \\ 0 & 0 & 0 & 0 & 1 \end{pmatrix}, \ \mathbf{B} = \begin{pmatrix} b'_{11} & b'_{12} & b'_{13} & b'_{14} & b'_{15} \\ b'_{21} & b'_{22} & b'_{23} & b'_{24} & b'_{25} \\ b'_{31} & b'_{32} & b'_{33} & b'_{34} & b'_{35} \\ \omega_0/2 & -\omega_0/2 & 0 & 0 & 0 \\ 0 & \omega_0/2 & -\omega_0/2 & 0 & 0 \end{pmatrix},$$

$\overline{\varepsilon} = \begin{pmatrix} \overline{\varepsilon}_1 & \overline{\varepsilon}_2 & \overline{\varepsilon}_3 & \overline{\varepsilon}_4 & \overline{\varepsilon}_5 \end{pmatrix}^{\mathrm{T}}, \dot{\overline{\varepsilon}} = \begin{pmatrix} \dot{\overline{\varepsilon}}_1 & \dot{\overline{\varepsilon}}_2 & \dot{\overline{\varepsilon}}_3 & \dot{\overline{\varepsilon}}_4 & \dot{\overline{\varepsilon}}_5 \end{pmatrix}^{\mathrm{T}}, \boldsymbol{\upsilon} = \begin{pmatrix} \upsilon_1 & \upsilon_2 & \upsilon_3 & 0 & 0 \end{pmatrix}^{\mathrm{T}}$. The items a'_{ij}, b'_{ij} and υ_i in Eq. (8) are presented in Appendix B.

The electromagnetic torque in Eq. (6) can be expressed as

$$\overline{T}_{ei} = T_{e0i} - k_{e0i}\overline{\varepsilon}_i \ (i = 1, 2, 3) \tag{9}$$

where, $T_{e0i} = f_i\omega_0 + m_i r^2 \omega_0 \kappa_i \ (i = 1, 2, 3)$ and k_{e0i} can be derived from literature[25]. T_{e0i} is painted as Fig. 5. When the three ERs reach the steady synchronization state, the non-linear parameters $p = q = s = 1$ and the small parameters $\varepsilon_1 = \varepsilon_2 = \varepsilon_3 = 0$, $\dot{\varepsilon}_1 = \dot{\varepsilon}_2 = \dot{\varepsilon}_3 = 0$. The synchronous condition of three ERs can be represented as Eq. (10).

$$|T_{e0i}| \le T_{eNi} \ (i = 1, 2, 3) \tag{10}$$

where, $T_{eNi} \ (i = 1, 2, 3)$ are respectively the rated electromagnetic torque of three motors. When the vibrating system satisfies the synchronization criterion, $\boldsymbol{\upsilon} = 0$. Equation (8) can be simplified as

$$\mathbf{A}\dot{\overline{\boldsymbol{\varepsilon}}} = \mathbf{B}\overline{\boldsymbol{\varepsilon}} \tag{11}$$

Because matrix $\mathbf{A}$ is a non-singular matrix, if the determinant $|A|$ of matrix A dose not equal to zero, the matrix $\mathbf{A}$ is an invertible matrix. Thus, Eq. (11) can be expressed as

$$\dot{\overline{\boldsymbol{\varepsilon}}} = \mathbf{D}\overline{\boldsymbol{\varepsilon}} \tag{12}$$

where, $\mathbf{D} = \mathbf{A}^{-1}\mathbf{B}$. The characteristic equation in Eq. (12) can be obtained by $\det(\lambda\mathbf{I} - \mathbf{D}) = 0$.

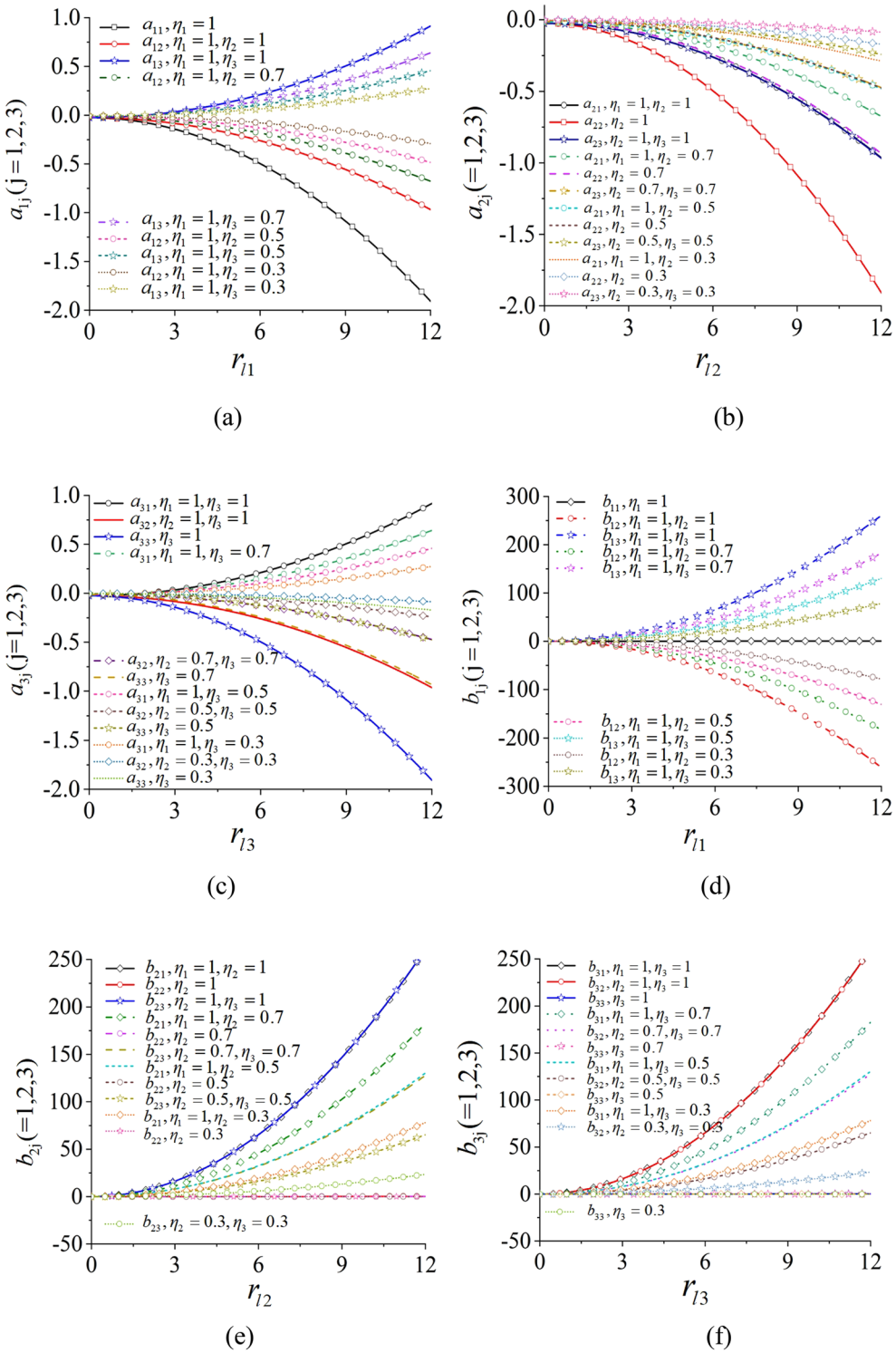

Figure 4. The parameters a_{ij} and b_{ij} with the relationship of r_l in the situation $\omega_0 = 80$ rad/s.

$$\lambda^5 + d_1\lambda^4 + d_2\lambda^3 + d_3\lambda^2 + d_4\lambda^1 + d_5 = 0 \tag{13}$$

$d_j\left(j = 1, 2, 3, 4, 5\right)$ are the coefficient items while λ represents the eigenvalue in Eq. (13). The parameters $d_j\,(j = 1, 2, 3, 4, 5)$ are given in Appendix C. When the characteristic equation satisfies the Hurwitz conditions in Eq. (14), all the real roots of eigenvalues exist on the left of coordinate (which means to be the negative real roots), the synchronous state of the vibrating system is stable. Otherwise, is unstable.

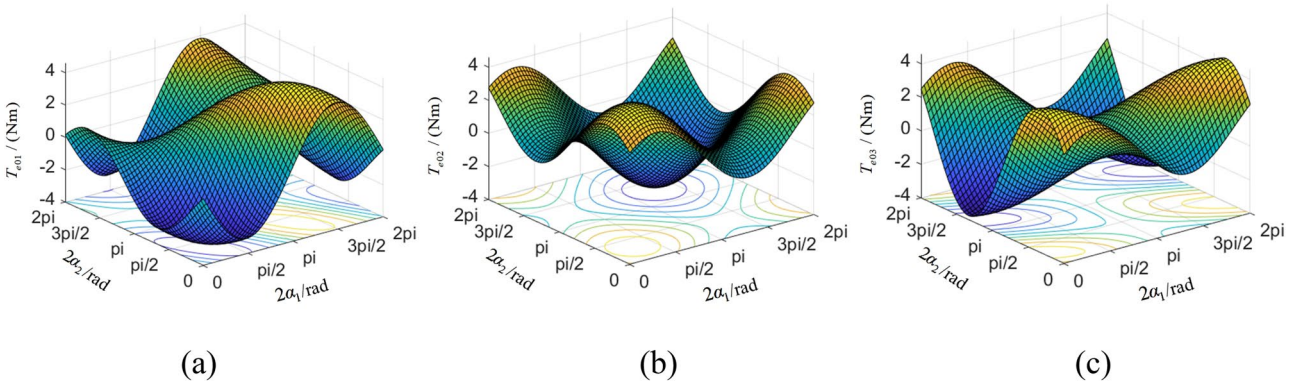

Figure 5. The electromagnetic torque of three motors.

$$\begin{cases} d_1 > 0, \\ d_5 > 0, \\ d_1 d_2 - d_3 > 0, \\ d_1 d_2 d_3 - d_3^2 - d_1^2 d_4 + d_1 d_5 > 0, \\ d_1 d_2 d_3 d_4 - d_1^2 d_4^2 - d_1 d_5 d_2^2 + 2 d_1 d_4 d_5 + d_2 d_3 d_5 - d_3^2 d_4 - d_5^2 > 0 \end{cases} \tag{14}$$

Design and theoretical analysis of the controlling system

Controller design of the controlling system

In this controlling scheme, a master–slave controlling strategy is introduced in the controlling system as shown in Fig. 6. ω_t as an input target speed is given into the master motor which is named motor 1. The output speed of motor 1 is divided into three functions. One is feedback to the initial speed to promote the accuracy of the motor speed. Another is as an input variable to realize the controlling strategy by the adaptive fuzzy PID method. In the meanwhile, it is converted to the speeds of motor 2 and 3. The other is changed to the phase through an integrate method and then transferred to the dynamical model. The processes of motor 2 and 3 are similar with motor 1's.

The fuzzy logic model is consisted of two input variables and three output variables. The two input variables are respectively the error e and the change rate of error ec. The three output variables are respectively the proportionality coefficient k_p, integral coefficient k_I and differential coefficient k_D. According to the usual fuzzy rules table, the output variables can be obtained through Eqs. (15) with forty-nine rules which are established in this section.

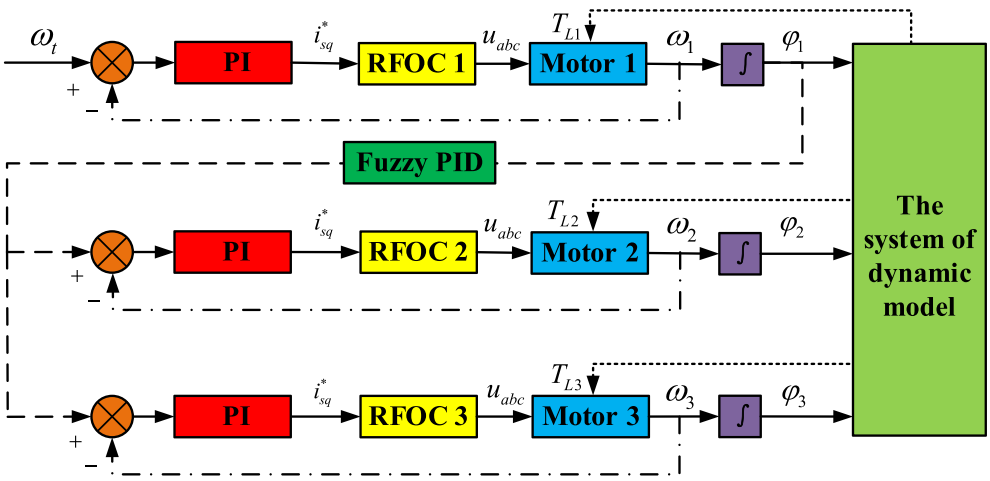

Figure 6. Framework diagram of the controlling system.

$$K_\iota = \frac{\left[\sum_{j=1}^{49} \mu_{K_{ij}}(e, ec) \times K_{ij}\right]}{\sum_{j=1}^{49} \mu_{K_{ij}}(e, ec)} \quad (\iota = P, I, D) \tag{15}$$

Theoretical analysis of the controlling system

Because the controlling method is applied in this article, the stability of the controlling method should be analyzed. Choosing the speed as the state variable, it can be expressed as $\omega = \dot{\varphi}$. And then, Eq. (2) can be derived as

$$J_i\dot{\omega}_i + f_i\omega_i = K_{T_i}u_i - W_i \ (i = 1, 2, 3) \tag{16}$$

$K_{T_i}u_i$ is introduced in the dynamical equation to replace the electromagnetic torque. Where, K_{T_i} is represented as the constant of the electromagnetic torque, $K_{Ti} = L_{mi}\phi_{rdi}/L_{ri}$, while u_i is considered as the controlling variable i^*_{qsi}. W_i replaces the load torque which is the uncertain loads in this section, $W_i = T_{Li}$. Set e as the speed error of the motor and then it can be expressed as the difference between the target speed and the actual speed in Eq. (17).

$$e = \omega_t - \omega \tag{17}$$

Thus, the tracing error $\boldsymbol{E}$ can be given as a column vector, $\mathbf{E} = [e, \dot{e}]^{\mathrm{T}}$. Because u_i is the controlling variable, the controlling law is defined as

$$u = J/K_T\left[-\hat{f}(x|\theta_f) + \dot{\omega}_t + \mathbf{K}^{\mathrm{T}}\mathbf{E} + (f\omega - W)/J\right] \tag{18}$$

$\boldsymbol{K}$ is composed of the parameters k_p and k_I, $\mathbf{K} = [k_p, k_I]^{\mathrm{T}}$. The weight coefficient θ_f in the function $\hat{f}(x)$ can be expressed as $\hat{f}(x|\theta_f) = \theta_f^{\mathrm{T}}\boldsymbol{\xi}(x)$. Where, $\boldsymbol{\xi}(x)$ is a fuzzy vector. Then the adaptive law of the fuzzy system is represented as

$$\dot{\theta}_f = -\gamma E^{\mathrm{T}}\mathrm{P}b\boldsymbol{\xi}(x) \tag{19}$$

γ is a positive constant and $\mathbf{P}$ is a positive definite matrix.

Taking Eq. (18) into Eq. (16), the dynamical equation with closed loop of the fuzzy controlling system can be expressed as

$$\dot{\mathrm{E}} = \boldsymbol{\Lambda}\mathrm{E} + \mathrm{b}\left[\hat{f}(x|\theta_f) - f(x)\right] \tag{20}$$

where, $\boldsymbol{\Lambda} = \begin{pmatrix} 0 & 1 \\ -k_p & -k_I \end{pmatrix}$, $\mathbf{b} = \begin{pmatrix} 0 \\ 1 \end{pmatrix}$.

To guarantee the boundedness of the weight coefficient θ_f, the optimal weight coefficient θ_f^* is introduced in the controlling system with a convex set Ω_f which contains θ_f, $\theta_f \in \Omega_f$. Thus, θ_f^* is constructed as

$$\theta_f^* = \arg\min_{\theta_f \in \Omega_f}\left[\sup|\hat{f}(x|\theta_f) - f(x)|\right] \tag{21}$$

Taking Eq. (19) and (21) into Eq. (20), the closed dynamical equation of the fuzzy system can be derived as

$$\dot{E} = \boldsymbol{\Lambda}E + b\left[(\theta_f - \theta_f^*)^{\mathrm{T}}\xi(x) + \Delta\right] \tag{22}$$

Δ is defined as the minimum approximation error and is expressed as $\Delta = \hat{f}(x|\theta_f^*) - f(x)$. To accord the adaptive law with the condition of the fuzzy system, the difference between the tracing error $\boldsymbol{E}$ and the parameter error $\theta_f - \theta_f^*$ should be minimum. So, a Lyapunov function is defined as

$$V = E^{\mathrm{T}}\mathbf{P}E/2 + (\theta_f - \theta_f^*)^{\mathrm{T}}(\theta_f - \theta_f^*)/(2\gamma) \tag{23}$$

γ is a positive constant. Through introducing a positive definite matrix $\mathbf{Q}$ with second order, the Lyapunov equation should be satisfied with matrix $\mathbf{P}$.

$$\boldsymbol{\Lambda}^{\mathrm{T}}\mathbf{P} + \mathbf{P}\mathbf{A} = -\mathbf{Q} \tag{24}$$

To certify the stability of Lyapunov function, the Lyapunov function in Eq. (23) is divided into two parts. One is $V_1 = E^{\mathrm{T}}\mathbf{P}E/2$, the other is $\mathbf{V}_2 = (\theta_f - \theta_f^*)^{\mathrm{T}}(\theta_f - \theta_f^*)/(2\gamma)$. According to the Lyapunov criterion, the derivation of $\boldsymbol{V}_1$ and $\boldsymbol{V}_2$ should be obtained, which are respectively $\dot{V}_1 = -E^{\mathrm{T}}\mathbf{Q}E/2 + (\theta_f - \theta_f^*)^{\mathrm{T}}E^{\mathrm{T}}\mathbf{P}b\xi(x) + E^{\mathrm{T}}\mathbf{P}b\Delta$ and $\dot{\mathbf{V}}_2 = (\theta_f - \theta_f^*)^{\mathrm{T}}\dot{\theta}_f/\gamma$. Thus, the derivate of Eq. (23) can be expressed as $\dot{\mathbf{V}} = \dot{\mathbf{V}}_1 + \dot{\mathbf{V}}_2 = -\mathrm{E}^{\mathrm{T}}Q\mathbf{E}/2 + \mathbf{E}^{\mathrm{T}}P\mathbf{b}\Delta$. Because of $-\mathrm{E}^{\mathrm{T}}Q\mathbf{E}/2 \leq 0$, only if the appropriate parameter Δ is chosen, $\dot{\mathbf{V}} \leq 0$ can be obtained. According to LaSalle invariance principle, the controlling system is asymptotic stable. The stability of other motors' speed error and the stability of phase error can be acquired with the method above.

Results analysis and discussions

In this section, numerical simulation results corresponding to the dynamical model of Fig. 1 are illustrated. And then, some experiment results are given to verify the simulation results. The feature of vibrating system is discussed.

Numerical simulation of self-synchronization and controlled synchronization

In Fig. 7, the simulation result of the self-synchronization with three ERs are presented. Figure 7a shows the speed of three motors. With the method of constant voltage frequency ratio, the speeds of three motors fluctuate around 60.02 rad/s which can be realized to reach the synchronous speeds. However, the phase differences between motor 1 and 2 with motor 2 and 3 are separately about 108.5° and 119.5° in Fig. 7b. The result illustrates that the vibrating system obviously can't reach the synchronous state with zero phase difference which is needed in the engineering. From Fig. 7c, it can be known that the amplitude of the vibrating system is counteracted due to the phase differences in Fig. 7b. Thus, the vibrating system appears an angle of oscillation with 0.02° in Fig. 7d. From the results in Fig. 7, it can be concluded that the vibrating system can't realize the synchronous state with zero phase difference. And then, the trajectory of the rigid body can't meet the engineering acquirements.

To solve this problem, the fuzzy PID method is introduced in the self-synchronization motion to realize the synchronous state with zero phase difference. From Fig. 8a, the speeds of three motors are all about 60 rad/s which equal to the target speed. Figure 8b demonstrates that the phase differences between motor 1 and 2 with motor 1 and 3 are both approximate to 0. And this result represents that the three ERs realize the controlled synchronization motion. In Fig. 8c, values of the torque load are between 0 and 0.12. These values are less than the absolute values of the electromagnetic torque. Thus, the three motor can operate normally and won't appear the phenomenon of motor blocking. From Fig. 8d,f, the results illustrate that the amplitudes of three ERs are superimposed and the angle of swing of the vibrating system is very small. The vibrating system realizes the controlled synchronization motion and the elliptical trace which is needed in the engineering. To expound the feature of distance between motor 1 and 2, the distance is expanded from center to the sides which is shown in Fig. 9. According to Fig. 9, the speeds and phase differences are both similar with them in Fig. 8. However, the torque loads of three motors enlarge in Fig. 9c due to the increasing of the swing angle in Fig. 9e. The results indicate that although the parameters l_1 and l_2 increase with increasing the distance between motor 1 and 2, this change has little influence on the controlled synchronization motion. Because the stable controlling method

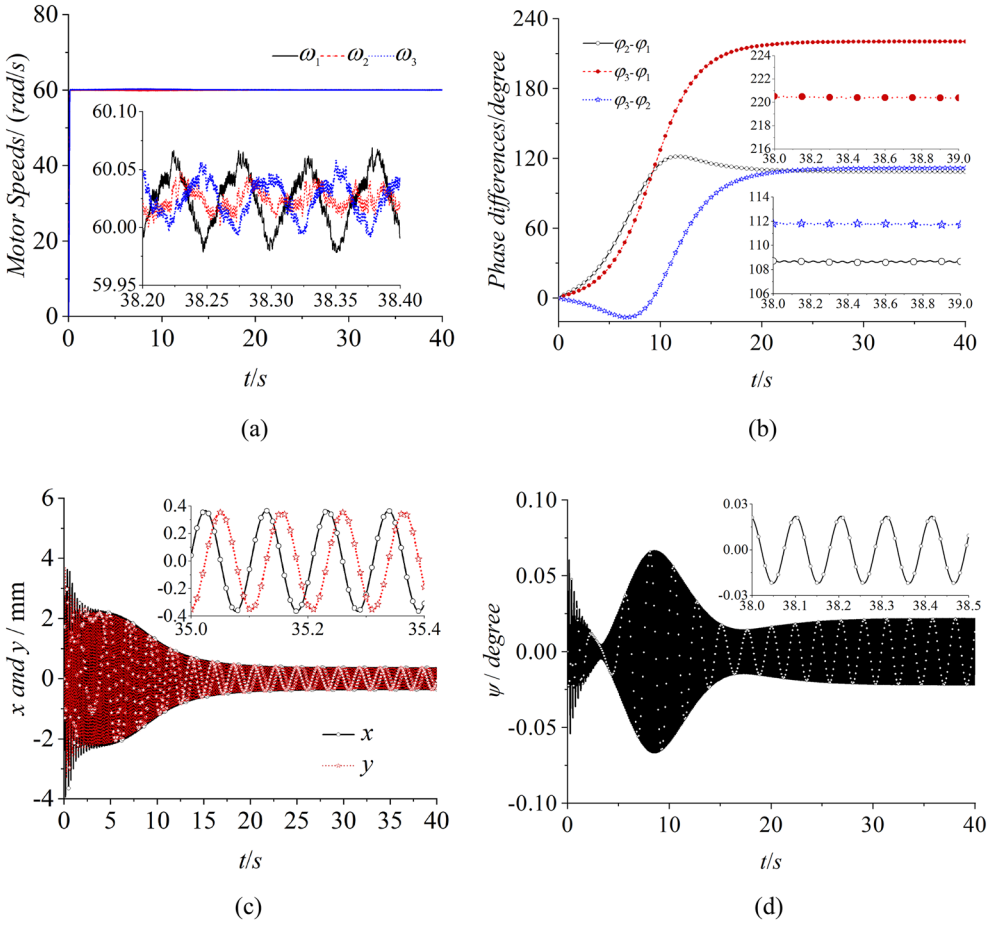

Figure 7. Self-synchronization with three ERs, α_0=0, $\eta_1 = \eta_2 = \eta_3 = 1$.

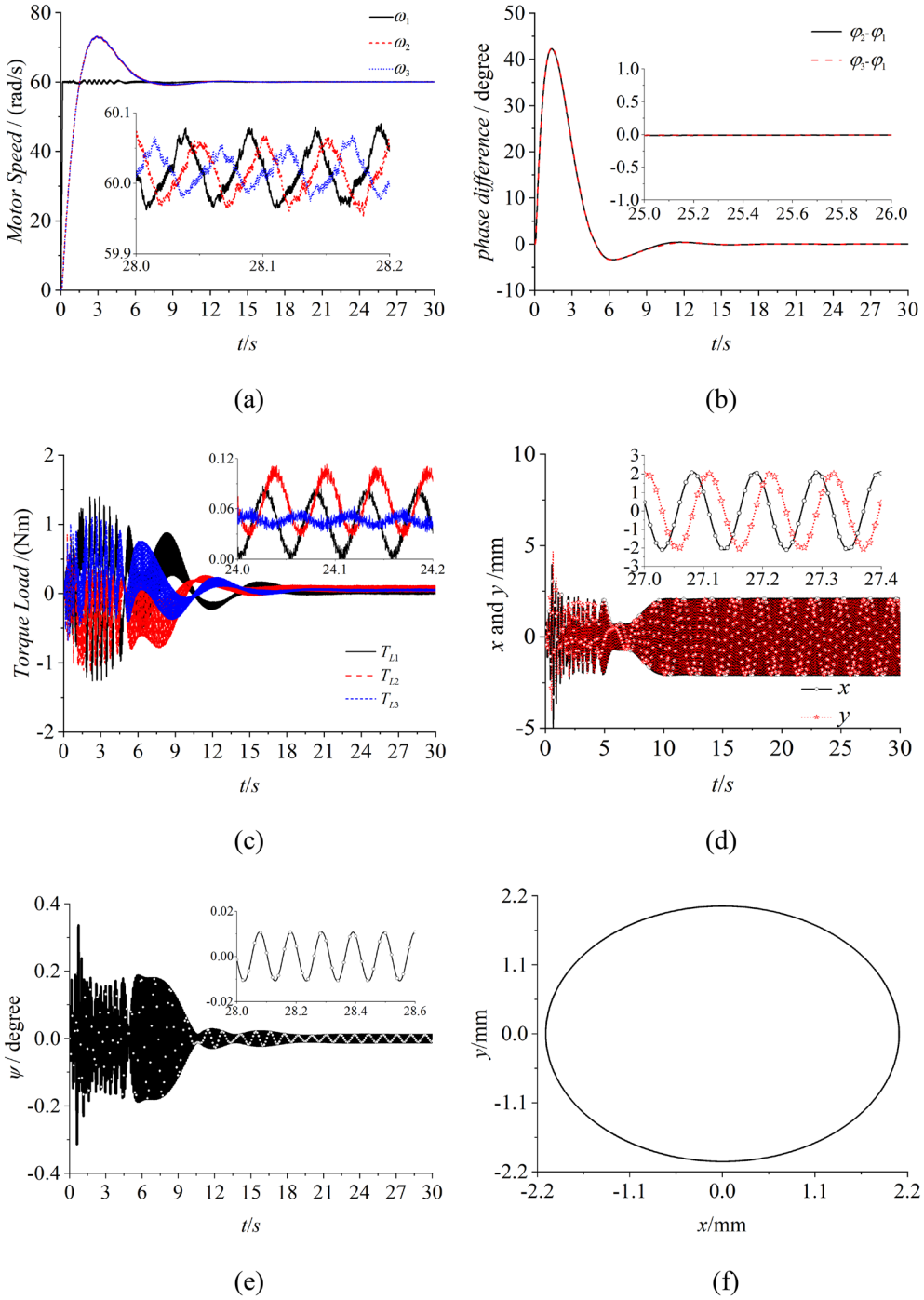

Figure 8. Controlled synchronization with three ERs, α_0=0, $\eta_1 = \eta_2 = \eta_3 = 1, l_1 = l_2 = 0.32m, l_3 = 0.3m$, (motor 1 and 2 approach the y axis).

changes the intrinsic dynamical feature of the vibrating system. Thus, to realize the miniaturization of the vibrating system, the parameters in Fig. 8 are more suitable for the engineering. This is the reason that the vibrating system is in a circular distribution rather than one straight line.

Experimental verification of self-synchronization and controlled synchronization

To certify the correctness of the proposed theory and the consistency with numerical simulation, some experiments of self-synchronization and controlled synchronization are given. The experimental facilities are firstly listed in Fig. 10 which illuminates the experimental procedure in the meanwhile. In this experiment, the frequencies of three inductor motors are respectively set as 35 Hz through three convertors. Through the calculation conversion, the speeds of three motors can be calculated as 73.2 rad/s which can be recognized as the theorical value. In Fig. 11a, the speeds of three motors all have a large fluctuation around 73 rad/s. Due to the existence of

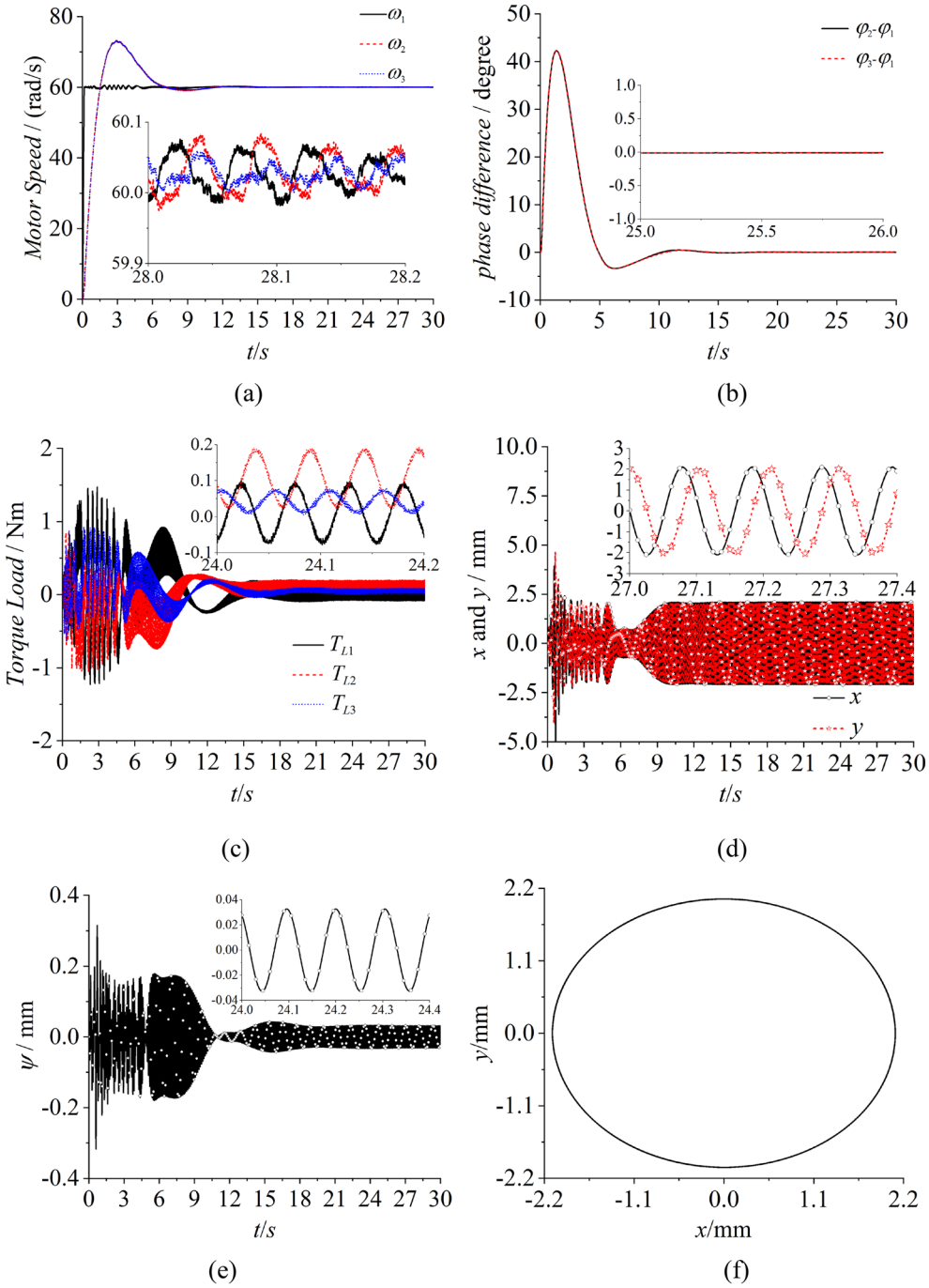

Figure 9. Controlled synchronization with three ERs, α_0=0, $\eta_1 = \eta_2 = \eta_3 = 1, l_1 = l_2 = 0.45m, l_3 = 0.3m$, (motor 1 and 2 approach both sides of the rigid body).

the error in the experiment, this result can be recognized to realize the synchronous speed. In Fig. 11b, the phase difference between motor 1 and 2 is about 127°, and this result is similar with the result in Fig. 7b. The same result can be obtained from the phase difference between motor 1 and 3. From Fig. 11c,e, the results indicates that the amplitude responses of three directions are all counteracted. Thus, the experimental result is consistence with the numerical simulation result of the self-synchronization. Figures 12 and 13 both represent the experimental results of the controlled synchronization motion and are respectively responses to the simulation results in Figs. 8 and 9. With the controlling method, the speeds of three motors exist less fluctuation. The phase differences can be considered small enough to realize the controlled synchronization motion. As shown from (d) to (g) in Figs. 12 and 13, the responses amplitudes in three directions are all in superposition state and the values are approximately the same. This result adequately represents that the vibrating system can realize the elliptic

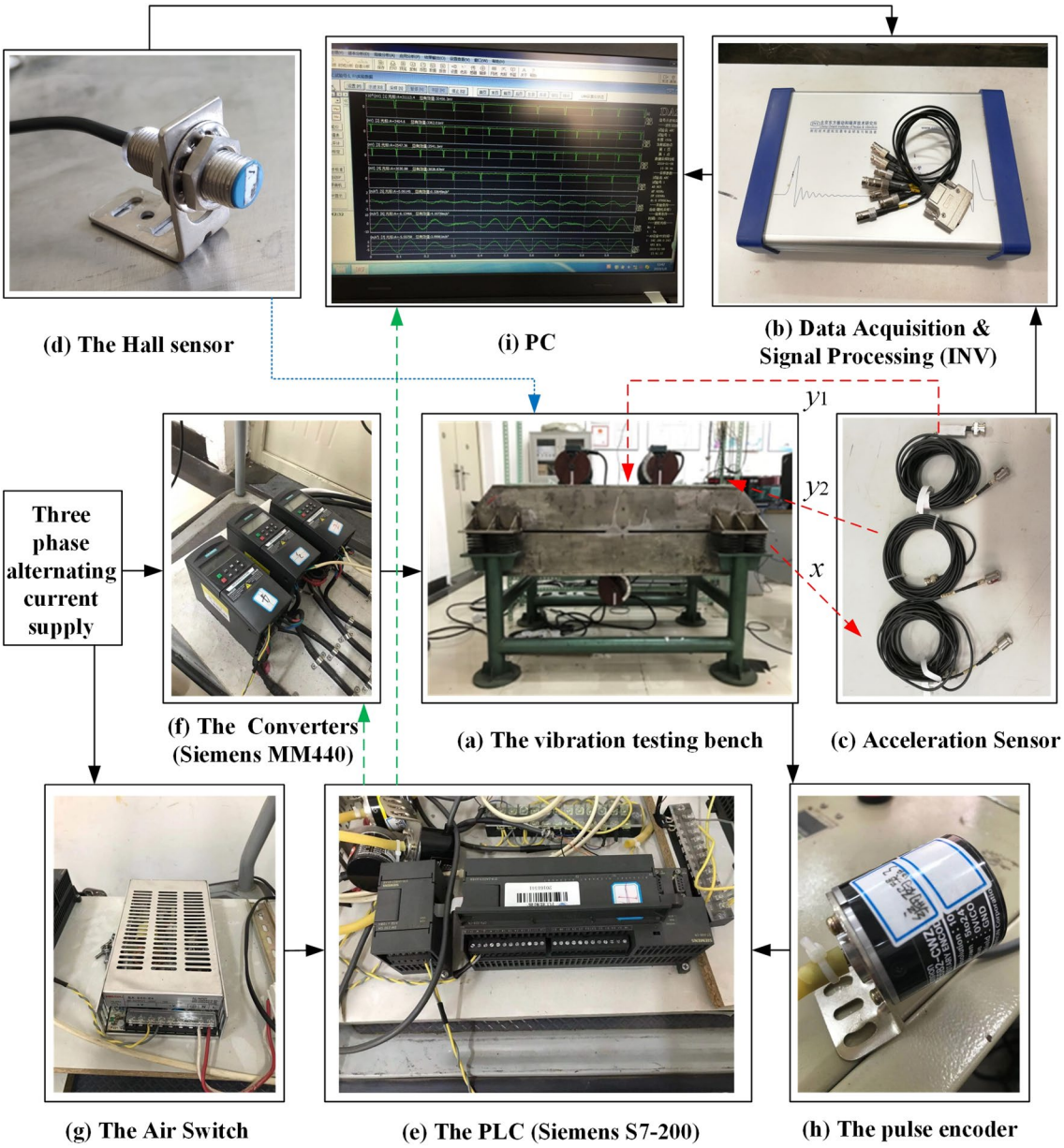

Figure 10. Experimental facilities.

motion trace. Therefore, the experimental results are consistent with the numerical results and the effectiveness and correctness of the theorical method are verified.

Conclusions

This article investigates controlled synchronization of three co-rotating exciters based on a circular distribution in a vibratory system. Through the theorical feature analysis, the results indicate that the self-synchronization motion is depended the parameter of η_i and l_i. When l_i can't meet the condition of zero phase difference in the self-synchronization motion, the ellipse motion trace in the vibrating system can't be realized. Therefore, the stability of the vibrating system depends on the controlling method and suitable controlling strategy in the controlled synchronization motion which can realize the ellipse motion trace in the vibrating system. Compared with the former researches, this article adopts a circle distribution in the dynamical model. It can further reduce the structure size of the vibrating system, which is the purpose of using the controlled synchronization instead of the self-synchronization. In the meanwhile, an adaptive fuzzy PID method is introduced. Because this method can be independent to the dynamical model and the parameter PID don't need to be founded with lots of time compared with the former methods.

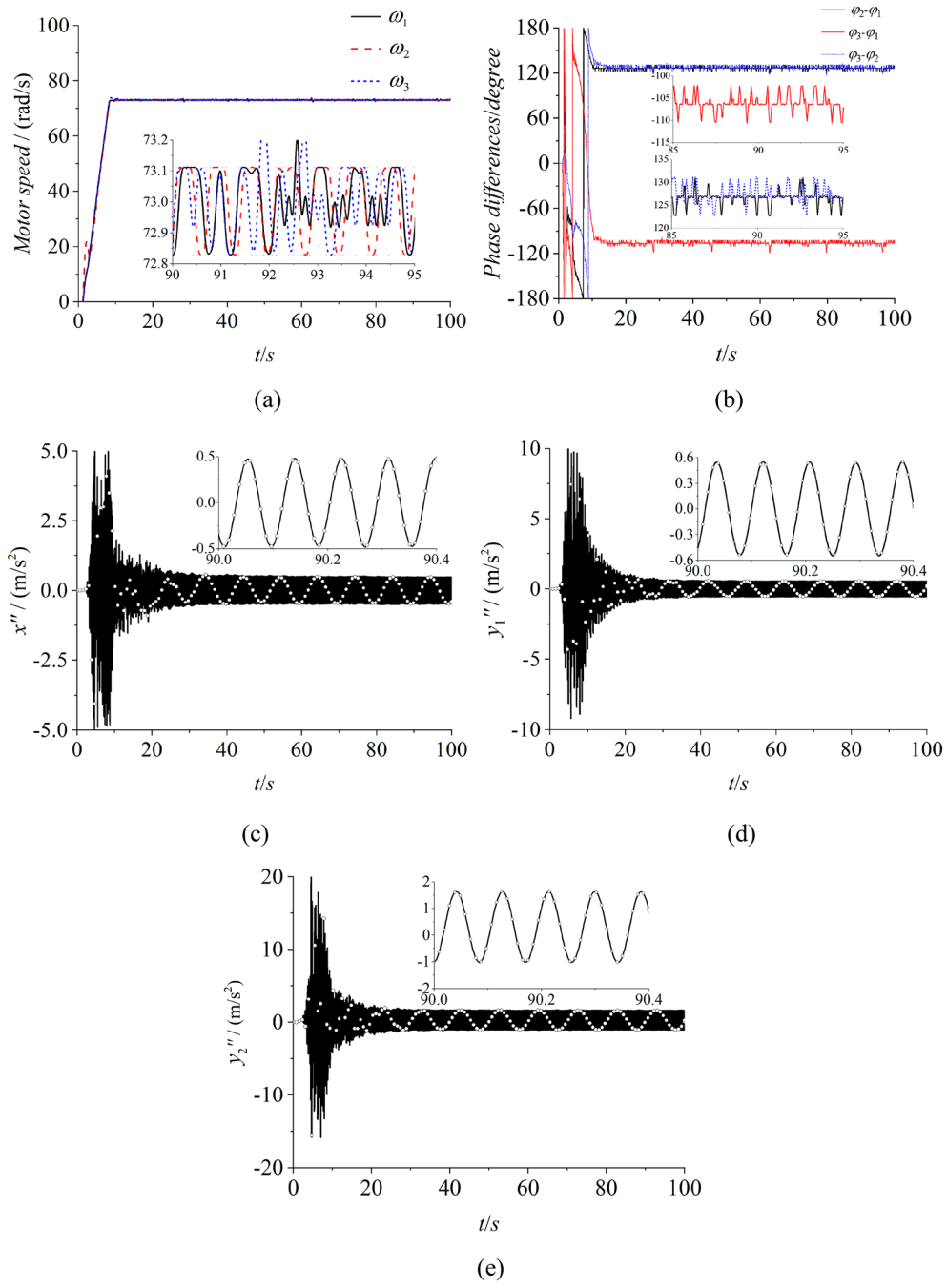

Figure 11. Experiment of self-synchronization with three ERs, α_0=0, $\eta_1 = \eta_2 = \eta_3 = 1$.

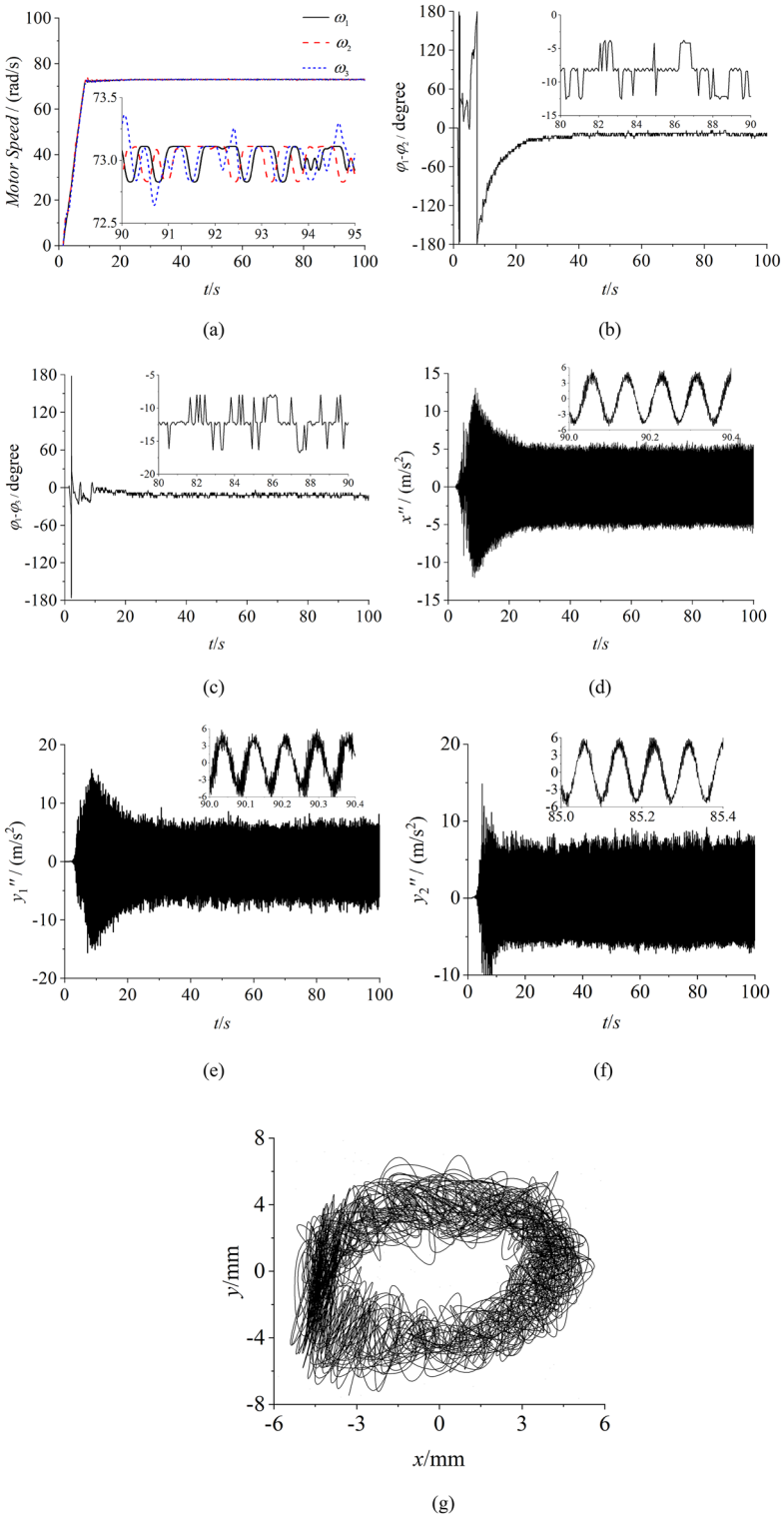

Figure 12. Experiment of controlled synchronization with three ERs, α_0=0, $\eta_1 = \eta_2 = \eta_3 = 1$ (motor 1 and 2 approach the *y* axis). (**a**) speeds, (**b**) phase difference between motor 1 and 2, (**c**) phase differences between motor 1 and 3, (**d**) response in the x direction, (**e**) response in the y1 direction, (**f**) response in the y2 direction, (**g**) The motion trace of the rigid body .

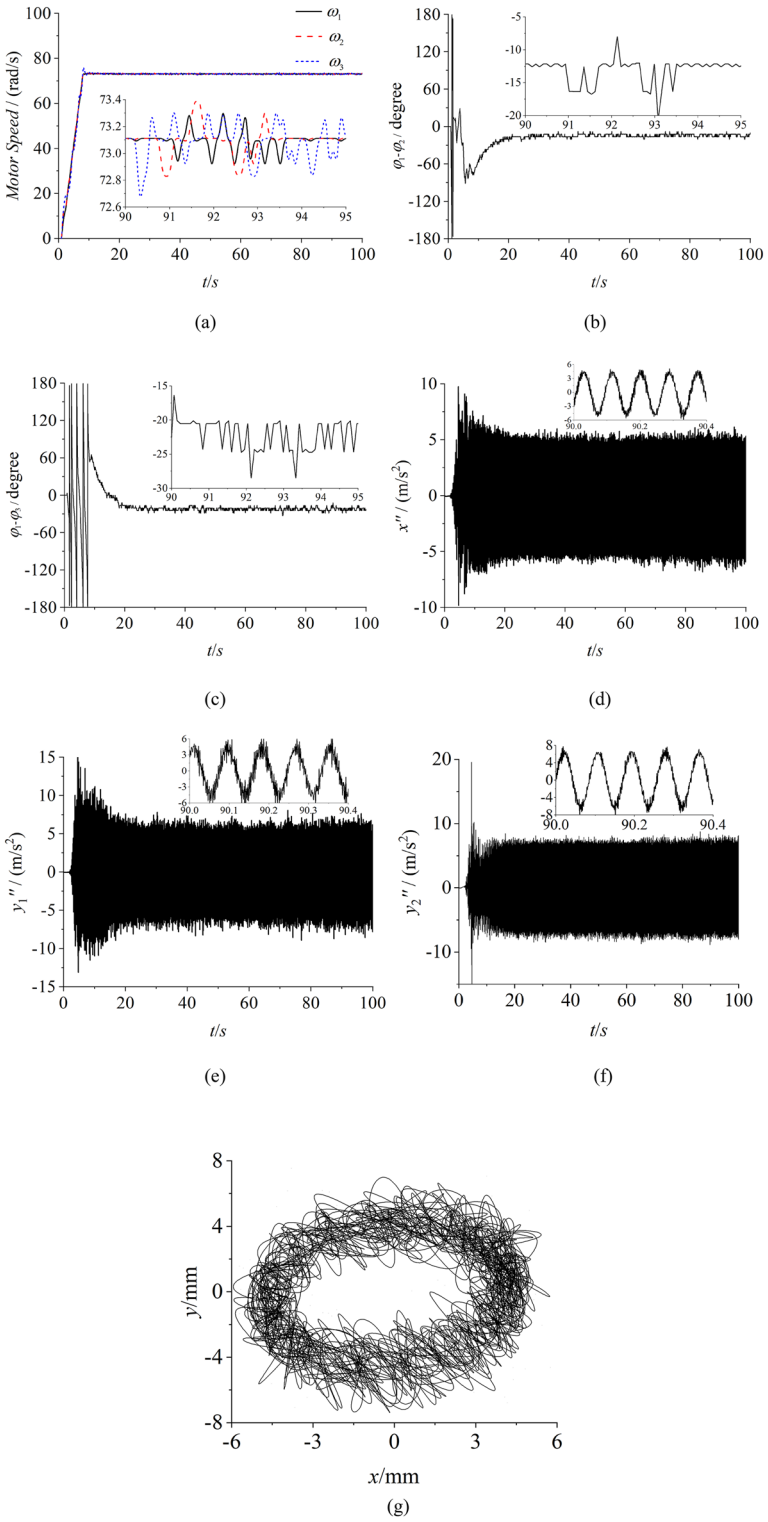

Figure 13. Experiment of controlled synchronization with three ERs, α_0=0, $\eta_1 = \eta_2 = \eta_3 = 1$ (motor 1 and 2 approach both sides of the rigid body). (**a**) speeds, (**b**) phase difference between motor 1 and 2, (**c**) phase differences between motor 1 and 3, (**d**) response in the x direction, (**e**) response in the y1 direction, (**f**) response in the y2 direction, (**g**) The motion trace of the rigid body

Data availability

The datasets generated during the current study are available from the corresponding/first author on reasonable request.

Received: 4 January 2024; Accepted: 26 February 2024
Published online: 29 February 2024

References

1. Wen, B. C., Fan, J., Zhao, C. Y. & Xiong, W. L. *Vibratory synchronization and controlled synchronization in engineering[M]* (Science Press, 2009).
2. Gallo, L. *et al.* Synchronization induced by directed higher-order interactions. *Commun. Phys.* **5**(1), 263 (2022).
3. Djanan, A. A. N., Nbendjo, B. R. N. & Woafo, P. Self-synchronization of two motors on a rectangular plate and reduction of vibration. *J. Vib. Control* **21**(11), 2114–2123 (2015).
4. Blekhman, I. I. & Sorokin, V. S. On the seperation of fast and show motion in mechanical system with high-frequency modulation of the dissipation coefficient. *J. Sound Vib.* **329**(3), 4936–4949 (2010).
5. Blekhman, I. I. & Yaroshevich, N. P. Extension of the domain of applicability of the integral stability criterion (extremum property) in synchronization problem. *J. Appl. Math. Mech.* **68**(2), 839–846 (2004).
6. Inoue Junki ch. On the self-synchronization of mechanical vibrators: Part 3, forced frictional vibrations. *Bull. Jsme* **35**(274), 1242–1248 (2008).
7. Wen, B. C., Zhang, H., Liu, S. Y., He, Q. & Zhao, C. Y. Theory and techniques of vibrating machinery and their applications. *Sci. Press Beijing.* **27**(3), 54–61 (2010).
8. Zhao, C. Y., Zhu, H. T., Zhang, Y. M. & Wen, B. C. Synchronization of two coupled exciters in a vibrating system of spatial motion. *Acta. Mech. Sin.* **26**(3), 477–493 (2010).
9. Zhao, C. Y., Wen, B. C. & Zhang, X. L. Synchronization of the four identical unbalanced rotors in a vibrating system of plane motion. *Sci. China Technol. Sci.* **53**(2), 405–422 (2010).
10. Zhang, X. L., Gu, D. W., Yue, H. L., Li, M. & Wen, B. C. Synchronization and stability of a far-resonant vibrating system with three rollers driven by two vibrators. *Appl. Math. Model.* **91**, 261–279 (2021).
11. Zhang, X. L., Yue, H. L., Li, Z. M., Xu, J. L. & Wen, B. C. Stability and coupling dynamic characteristics of a vibrating system with one internal degree of freedom and two vibrators. *Mech. Syst. Signal Pr.* **143**, 106812 (2020).
12. Zhang, X. L., Zhang, X., Zhang, C., Wang, Z. H. & Wen, B. C. Double and triple-frequency synchronization and their stable states of the two co-rotating exciters in a vibrating mechanical system. *Mech. Syst. Signal Pr.* **154**, 107555 (2021).
13. Balthazar, J. M., Felix, J. L. P. & Brasil, R. Short comments on self-synchronization of two non-ideal sources supported by a flexible portal frame structure. *J. Vib. Control* **10**(12), 1739–1748 (2004).
14. Balthazar, J. M., Felix, J. L. P. & Brasil, R. M. Some comments on the numerical simulation of self-synchronization of four non-ideal exciters. *Appl. Math. Comput.* **164**(2), 615–625 (2005).
15. Kong, X. X., Zhang, X. L., Wen, B. C. & Wang, B. Synchronization analysis and control of three eccentric rotors in a vibrating system using adaptive sliding mode control algorithm. *Mech. Syst. Signal Process.* **72–73**, 432–450 (2016).
16. Kong, X. X., Li, W. J., Jiang, J., Dong, Z. X. & Wang, Z. Z. Dynamic characteristics of a simply supported elastic beam with three induction motors. *J. Sound Vib.* **520**, 116603 (2021).
17. Kong, X. X., Chen, C. Z. & Wen, B. C. Composite synchronization of three eccentric rotors driven by induction motors in a vibrating system. *Mech. Syst. Signal Process.* **102**, 158–179 (2018).
18. Perez-Pinal F.J. Calderon G., Araujo-Vargas I. Relative Coupling Strategy[C]. *IEEE International Conference on Electric Machines and Drives*, (2003).
19. Huang, Z. L., Zhang, Z. C., Wu, J., Wu, J. Z. & Sun, S. S. Frequency-multiplying synchronous control of the multiple counter-rotating exciters in vibration system. *J. Sound Vib.* **562**, 117852 (2023).
20. Huang, Z. L., Song, G. Q., Li, Y. M. & Sun, M. N. Synchronous control of two counter-rotating eccentric rotors in nonlinear coupling vibration system. *Mech. Syst. Signal Process.* **114**, 68–83 (2019).
21. Priyanka, E. B., Maheswari, C. & Thangavel, S. Online monitoring and control of flow rate in oil pipelines transportation system by using PLC based fuzzy-PID controller. *Flow Measur. Instrum.* **62**, 144–151 (2018).
22. Jia, L. & Liu, Z. L. Multifrequency composite synchronization of three inductor motors with the method of fixed speed ratio in a vibration system. *P. I. Mech. Eng. E J. Pro.* **237**, 254–268 (2023).
23. Jia, L., Wang, C. & Liu, Z. Multifrequency controlled synchronization of four inductor motors by the fixed frequency ratio method in a vibration system. *Sci. Rep.* **13**(1), 2467 (2023).
24. Luca, B., Gianantonio, M., Paolo, R. & Andrea, M. Z. Performance limitations in field-oriented control for asynchronnous machines with low resolution position sensing. *IEEE Trans. Control Syst. Technol.* **18**(3), 559–573 (2010).
25. Chen, J. *Mathematical Model and Speed Adjustment System of Alternating Motors* (Defense Press, 1989).

Acknowledgements

The author's research is supported by 2022 Liaoning Education department General Project (Project No.LJKMZ20220602). The APC was funded by the same funders.

Author contributions

L.J. wrote the article, Y.T. compiled the figures and tables, Z.L. conducted the simulation and led the experiments, and X.Z. checked the article.

Competing interests

The authors declare no competing interests.

Additional information

Supplementary Information The online version contains supplementary material available at https://doi.org/10.1038/s41598-024-55680-8.

Correspondence and requests for materials should be addressed to L.J.

Reprints and permissions information is available at www.nature.com/reprints.